Spatiotemporal variations of shallow very low frequency earthquake activity southeast off the Kii Peninsula, along the Nankai Trough, Japan

Shunsuke Takemura[1], Kazushige Obara[2], Katsuhiko Shiomi[3], and Satoru Baba[1]

[1]Earthquake Research Institute, the University of Tokyo
[2]Earthquake Research Institute, The University of Tokyo
[3]National Research Institute for Earth Science and Disaster Resilience

November 30, 2022

Abstract

Cross-correlation analysis was applied to long-term onshore broadband records from April 2004 to March 2021 to detect and relocate shallow very low frequency earthquakes (VLFEs) southeast off the Kii Peninsula, along the Nankai Trough, Japan. We then determined the moment rate functions of detected shallow VLFEs using the Monte Carlo-based simulated annealing method. According to this new comprehensive catalog, shallow VLFEs are widespread beneath the accretionary prism toe, but shallow VLFEs with large cumulative moments are localized around the western edge of the paleo-Zenisu ridge, which is subducted beneath southeast off the Kii Peninsula. This finding indicates that the subducted ridge causes heterogeneous structures and stress conditions that promote shallow slow earthquakes. The relocated shallow VLFE epicenters illustrated three major episodes characterized by a similar activity area and five minor episodes characterized by different areas. The three major episodes exhibited slow frontal migration with different initiation locations, directions, and speeds, as well as several rapid reverse migrations. Episodes of minor activity were distributed in different locations within part of the area of major activity. According to our results and the geometry of the plate boundary, we conclude that the subducted ridge also plays an important role in the activity area of shallow VLFE episodes. Different patterns of shallow VLFE migration could reflect temporal changes in the pore-fluid distribution or stress conditions of the plate boundary.

Hosted file

`2021_takemuraobarashiomibaba_si_v2.docx` available at https://authorea.com/users/539748/articles/607901-spatiotemporal-variations-of-shallow-very-low-frequency-earthquake-activity-southeast-off-the-kii-peninsula-along-the-nankai-trough-japan

Hosted file

`essoar.10507824.1.docx` available at https://authorea.com/users/539748/articles/607901-spatiotemporal-variations-of-shallow-very-low-frequency-earthquake-activity-southeast-off-the-kii-peninsula-along-the-nankai-trough-japan

Shunsuke TAKEMURA[1], Kazushige OBARA[1], Katsuhiko SHIOMI[2], Satoru BABA[1]

[1]Earthquake Research Institute, the University of Tokyo, 1-1-1 Yayoi, Bunkyo-ku, Tokyo, 113-0032, Japan.

[2]National Research Institute for Earth Science and Disaster Resilience, 3-1 Tennodai, Tsukuba, Ibaraki, 305-0006, Japan.

Corresponding author: Shunsuke TAKEMURA (shunsuke@eri.u-tokyo.ac.jp)

Key Points:

- We estimated the locations and moment rate functions of shallow very low frequency earthquakes that occurred near the Nankai Trough
- Large cumulative moments of shallow very low frequency earthquakes were concentrated in the region with the subducted oceanic ridge
- The migration of shallow very low frequency earthquakes exhibits various patterns in terms of initiation, migration direction, and area

Abstract

Cross-correlation analysis was applied to long-term onshore broadband records from April 2004 to March 2021 to detect and relocate shallow very low frequency earthquakes (VLFEs) southeast off the Kii Peninsula, along the Nankai Trough, Japan. We then determined the moment rate functions of detected shallow VLFEs using the Monte Carlo-based simulated annealing method. According to this new comprehensive catalog, shallow VLFEs are widespread beneath the accretionary prism toe, but shallow VLFEs with large cumulative moments are localized around the western edge of the paleo-Zenisu ridge, which is subducted beneath southeast off the Kii Peninsula. This finding indicates that the subducted ridge causes heterogeneous structures and stress conditions that promote shallow slow earthquakes. The relocated shallow VLFE epicenters illustrated three major episodes characterized by a similar activity area and five minor episodes characterized by different areas. The three major episodes exhibited slow frontal migration with different initiation locations, directions, and speeds, as well as several rapid reverse migrations. Episodes of minor activity were distributed in different locations within part of the area of major activity. According to our results and the geometry of the plate boundary, we conclude that the subducted ridge also plays an important role in the activity area of shallow VLFE episodes. Different patterns of shallow VLFE migration could reflect temporal changes in the pore-fluid distribution or stress conditions of the plate boundary.

Plain Language Summary

Our knowledge of the physical characteristics of shallow slow earthquakes, which may provide frictional properties on plate boundaries and preparation processes

of large interplate earthquakes, is still limited. Thus, we comprehensively analyzed shallow very low frequency earthquakes (VLFEs) southeast off the Kii Peninsula, in the Nankai subduction zone, where large tsunamigenic earthquakes have repeatedly occurred with intervals of approximately 100–200 years. We found that shallow VLFEs occurred around the western edge of the subducted oceanic ridge. We considered that this ridge causes complex stress and subsurface structures around the plate boundary and consequently promotes slow earthquake activity.

1 Introduction

In various subduction zones, megathrust earthquakes have repeatedly occurred at intervals of several hundred years as a result of accumulated shear stress caused by plate subduction. The stress accumulation and release processes on the plate boundary are important for the earthquake cycle and source physics. Slow earthquakes can release part of accumulated stress on the plate boundary. Slow earthquakes occur as slips on the plate boundary; however, their rupture durations are significantly longer than those of regular earthquakes with a similar magnitude (summarized in Ide et al., 2007; Obara & Kato, 2016). Slow and regular interplate earthquakes are separately distributed on the plate boundary (e.g., Baba et al., 2021; Dixon et al., 2014; Nishikawa et al., 2019; Plata-Martinez et al., 2021; Takemura, Okuwaki, et al., 2020; Vaca et al., 2018), reflecting the heterogeneous distribution of effective strength and stress conditions. Thus, studies of the source processes of both slow and regular interplate earthquakes are important for understanding and monitoring stress accumulation on the plate boundary.

Slow earthquakes occur on various timescales. Tectonic tremors and very low frequency earthquakes (VLFEs) are recorded at seismic stations in frequency ranges of 2–8 Hz and 0.02–0.05 Hz, respectively. The geodetic observations detect slow slip events (SSEs), with durations ranging from several days to several years. Spatiotemporal correlations among these various earthquake phenomena have also been reported, which are referred to as episodic tremor and slip (ETS; Hirose & Obara, 2006; Ito et al., 2007; Rogers & Dragert, 2003). Dense onshore seismic and geodetic observations have allowed us to analyze the source characteristics of deep slow earthquakes that occur around the deeper extensions of megathrust seismogenic zones. In Nankai and Cascadia subduction zones, various physical characteristics of deep slow earthquake sources have been reported (e.g., Bostock et al., 2015; Ide et al., 2008; Michel et al., 2019; Supino et al., 2020). Shallow slow earthquakes occur at shallower extensions of megathrust zones and are often considered possible triggers of megathrust earthquakes (e.g., Kato et al., 2012, 2016; Vaca et al., 2018; Voss et al., 2018). However, owing to the lack of long-term offshore observations and strong offshore heterogeneities around source regions, our knowledge of the characteristics of shallow slow earthquake sources is still limited. As such, a stable and accurate analysis of long-term observation records is required to discuss the characteristics of shallow slow earthquakes, which may provide key information on the shear

strength and structural conditions on shallow plate boundaries.

In this study, we investigate the source and migration characteristics of shallow VLFEs that occurred southeast off the Kii Peninsula, Japan (Figure 1) within 15–35 km from the Nankai Trough (deformation front). Along the Nankai Trough, megathrust earthquakes have repeatedly occurred at intervals of 100–200 years (e.g., Ando, 1975), and various shallow slow earthquake phenomena have been detected (e.g., Araki et al., 2017; Obara & Ito, 2005). Takemura, Noda, et al. (2019) revealed that shallow VLFEs tend to migrate in the regions surrounding the shear stress accumulation peaks on the Philippine Sea Plate boundary. However, they only detected and relocated shallow VLFEs during episodes that started from September 2004, March 2009, and April 2016. Thus, in this study, we comprehensively detect and relocate all shallow VLFEs from April 2004 to March 2021 (a period of 17 years). In addition, we estimate the moment rate functions of detected shallow VLFEs using Green's functions of the local three-dimensional (3D) model in order to determine their source characteristics. We also discuss the migration of shallow VLFEs.

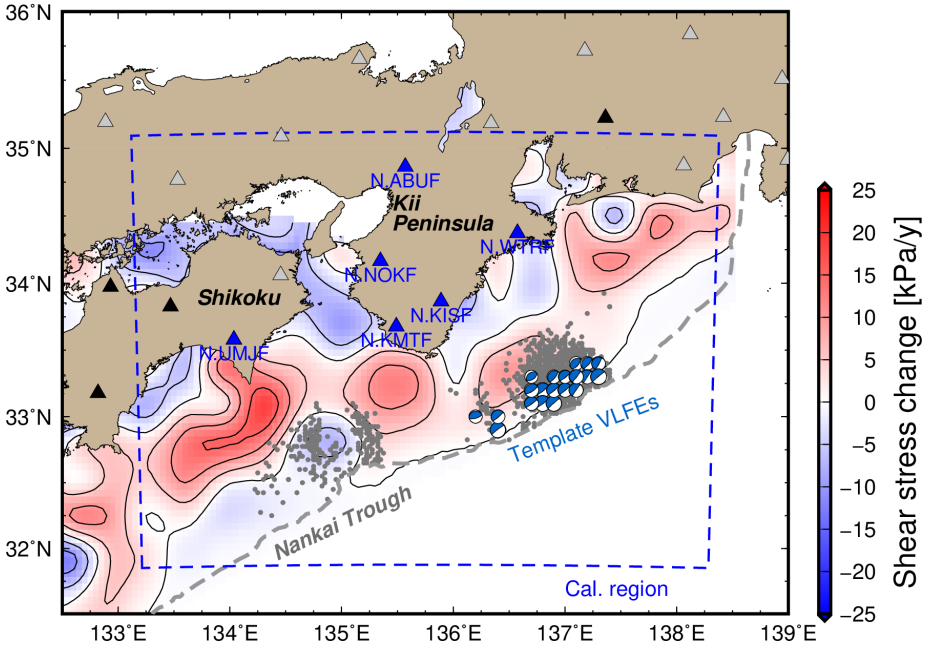

Figure 1. Map of the Nankai subduction zone. Gray circles are the epicenters of shallow VLFEs detected in our previous study (Takemura, Noda, et al., 2019). Blue focal spheres are the template shallow VLFEs, which are well-constrained centroid moment tensor solutions derived from Takemura, Matsuzawa, et al. (2019). Triangles are the F-net stations. Stations with black and blue filled triangles were used in the template matching and relocation analysis. Stations represented by gray triangles were not used in the analysis. Estimates of moment rate functions for the detected VLFEs were derived from data at the blue filled

triangles. Blue dashed rectangle represents the horizontal calculation region for Green's functions. Background color represents the shear stress change rate on the plate boundary caused by the subduction of the Philippine Sea Plate (Noda et al., 2018).

2 Data and Methods

To detect shallow VLFEs southeast off the Kii Peninsula in the Nankai subduction zone, we used three-component continuous velocity records at full-range seismogram network (F-net) broadband stations from April 2004 to March 2021. F-net is operated by the National Research Institute for Earth Science and Disaster Resilience (NIED; Aoi et al., 2020). Although data from the Dense Oceanfloor Network system for Earthquakes and Tsunamis (DONET) has been available since August 2011, F-net covers a longer observation period. In particular, two large shallow VLFE episodes occurred in September 2004 and March 2009, prior to the deployment of DONET. Using the method of Takemura, Noda, et al. (2019), we performed template matching and relocation analysis of shallow VLFEs southeast off the Kii Peninsula. For the detection and moment rate function estimation, we selected the frequency band of 0.02–0.05 Hz to enhance small shallow VLFE signals and avoid the period bands of microseisms at onshore seismic stations (e.g., Nishida, 2017).

We then calculated the cross-correlation coefficients (CCs) between the filtered template and observed seismograms every 1 s. The blue focal spheres in Figure 1 show the template events of shallow VLFEs, whose template waveforms can be downloaded from the supporting information of Takemura, Noda, et al. (2019). Assuming 3.8 km/s as the propagation velocity of surface wave, the CCs at the stations were back-propagated to possible shallow VLFE epicenters, which were uniformly distributed at an interval of 0.025°. After averaging the CCs at the stations for each time and grid, we detected the events with average CCs 0.45 as shallow VLFE candidates. To avoid regular earthquakes and duplicate detections, we removed the local regular earthquakes listed in the unified hypocenter catalog of the Japan Meteorological Agency and selected a shallow VLFE candidate with the maximum CC every 60 s. Because of the station distribution, our method constrained the shallow VLFE epicenters along the strike direction (Figure 1bd of Takemura, Noda, et al., 2019). The cumulative number of detected shallow VLFEs over time is shown in Figure S1.

After detection and relocation, we estimated the moment rate functions of the detected shallow VLFEs using the Monte Carlo-based simulated annealing technique. Surface wave propagation from shallow VLFEs to F-net stations is significantly affected by the 3D heterogeneous structures of the accretionary prism, the Philippine Sea Plate, and seawater (e.g., Nakamura et al., 2015). Thus, we prepared Green's functions in the local 3D model via reciprocal calculations using an open-source seismic wave propagation code (OpenSWPC; Maeda et al., 2017). The simulation model covered an area of $360\times480\times80$ km^3 (blue dashed rectangle in Figure 1), discretized by grid intervals of 0.2 km in the horizontal direction and 0.1 km in the vertical direction. The assumed 3D velocity

model was constructed by combining the Japan Integrated Velocity Structure Model (JIVSM; Koketsu et al., 2012) and 1D velocity models beneath DONET stations (https://doi.org/10.5281/zenodo.4158946; Tonegawa et al., 2017). The detailed model construction process was described previously by Takemura et al. (2020). The possible source grids were similar to those in the relocation analysis. Each reciprocal calculation required 727 GB of computer memory and 2 h of computation time using 48-node hybrid (OpenMP/MPI) parallel computation on the Fujitsu PRIMERGY CX600M1/CX1640M1 (Oakforest-PACS) at the Information Technology Center, the University of Tokyo.

The moment rate function estimation procedure is as follows. The epicenter and depth were fixed at the location after VLFE relocation and the depth of the upper surface of the JIVSM Philippine Sea Plate. Because shallow VLFEs are characterized by low-angle thrust faulting (e.g., Sugioka et al., 2012; Takemura, Matsuzawa, et al., 2019), focal mechanisms were also fixed as low-angle thrust faulting constructed by the plate geometry of JIVSM and convergence directions of NUVEL-1A (DeMets et al., 2010). In this study, the moment rate function was constructed using a series of Küpper wavelets with a duration of 6 s. The synthetic velocity waveform $v_{ij}(t)$ from the j-th source grid to the i-th station can be written as follows:

$v_{\mathrm{ij}}(t) = A_0 \sum_{k=0}^{N_P-1} w_k^2 G_{\mathrm{ij}}(t - k\Delta t)$,
where G_{ij} is the Green's function of the j-th source with a unit 6-s Küpper wavelet, ${w_k}^2$ is the weight of the k-th Küpper wavelet, and t is the offset of each pulse (3 s). Non-negative conditions ${w_k}^2$ were imposed in our estimation. The parameter A_0 is the optimal relative amplitude estimated by fitting observed waveforms to synthetic waveforms based on variance reduction (Yabe et al., 2021). Using the observed waveform and amplitude-adjusted model seismogram v^{syn}, the objective function used in this analysis was

$E = \sum_i \sum_l \left| v_{\mathrm{ij}}^{\mathrm{obs}}(t_l + \tau) - v_{\mathrm{ij}}^{\mathrm{syn}}(t_l) \right|$
where is the delay time and the length of the time window is 200 s (t_l = 0–200 s). The parameters ${w_k}^2$ and were estimated via the Monte Carlo-based simulated annealing procedure. At each iteration step, w = 0.02 and = 0.5 s were perturbed for the source weights (w_k) and delay time ( ), respectively. According to shallow VLFE duration measurements derived from offshore broadband analysis (Sugioka et al., 2012), the number of source weight parameters was 40; thus, the maximum duration of the modeled moment rate function was 123 s. The parameters of the initial temperature ($T_0 = 3E_0$) and cooling rate (= 0.996) in the simulated annealing were similar to those in Tocheport et al. (2007). We initially assumed ${w_k}^2 = 1$, which could not reproduce the observed seismograms (Figure 2b). The annealing schedule at the k-th iteration was given by $T_k = {}^kT_0$. The perturbation at the k-th iteration with E_k (=E_k-E_{k-1}) < 0 was fully accepted. We also accepted the perturbation with E_k 0 and the probability of $P = \exp(-E_k/T_k)$ equal to less than , which is a random number between 0 and 1 at each iteration.

An example of the moment rate function estimation is shown in Figure 2. The gray line in Figure 2a represents the original estimate of the moment rate function via the simulated annealing method. Because our estimations were conducted using a frequency band of 0.02–0.05 Hz, longer duration small tail at times after about 30 s (i.e., the later part of the gray line in Figure 2a) may not contribute to the reproducibility of the observed seismograms for frequencies of 0.02–0.05 Hz. In addition, for cases with a low signal-to-noise ratio, our method might model reverberations of later weak surface waves within oceanic sediments and noise signals as a seismic moment release from the source. Therefore, to avoid misestimation of moment rate functions after the simulated annealing procedure, especially due to noise signals, we calculated the variance reductions (VRs) between observed and synthetic seismograms, which were constructed using N Küpper pulses. We adopted up to the N-th (N = 1–40) parameters, which achieved 90 % of the maximum VR (VR_m) for the simulated annealing result. The gray and blue lines in Figure 2a show the results of the original simulated annealing and optimal solutions, respectively. The synthetic seismograms obtained using the optimal solution reproduced the observed seismograms (Figure 2c). Although we adopted the solutions with 90 % of the VR_m in later discussions (Figures 3–7), we also tested other VR thresholds for 85 % and 95 % of the VR_m (Figures S2–S7).

After obtaining the optimal solution, we calculated the VR values between the observed and optimal syntenic seismograms. These VR values represent the goodness-of-fit factors for the optimal solutions. For shallow VLFEs with lower VRs ($<$ 30 %), the signals at onshore F-net stations can be weak compared to the noise signals; consequently, their durations might be misestimated due to low signal-to-noise ratio conditions. Therefore, in subsequent discussions of shallow VLFE activities, we discarded the results with VRs $<$ 30 %.

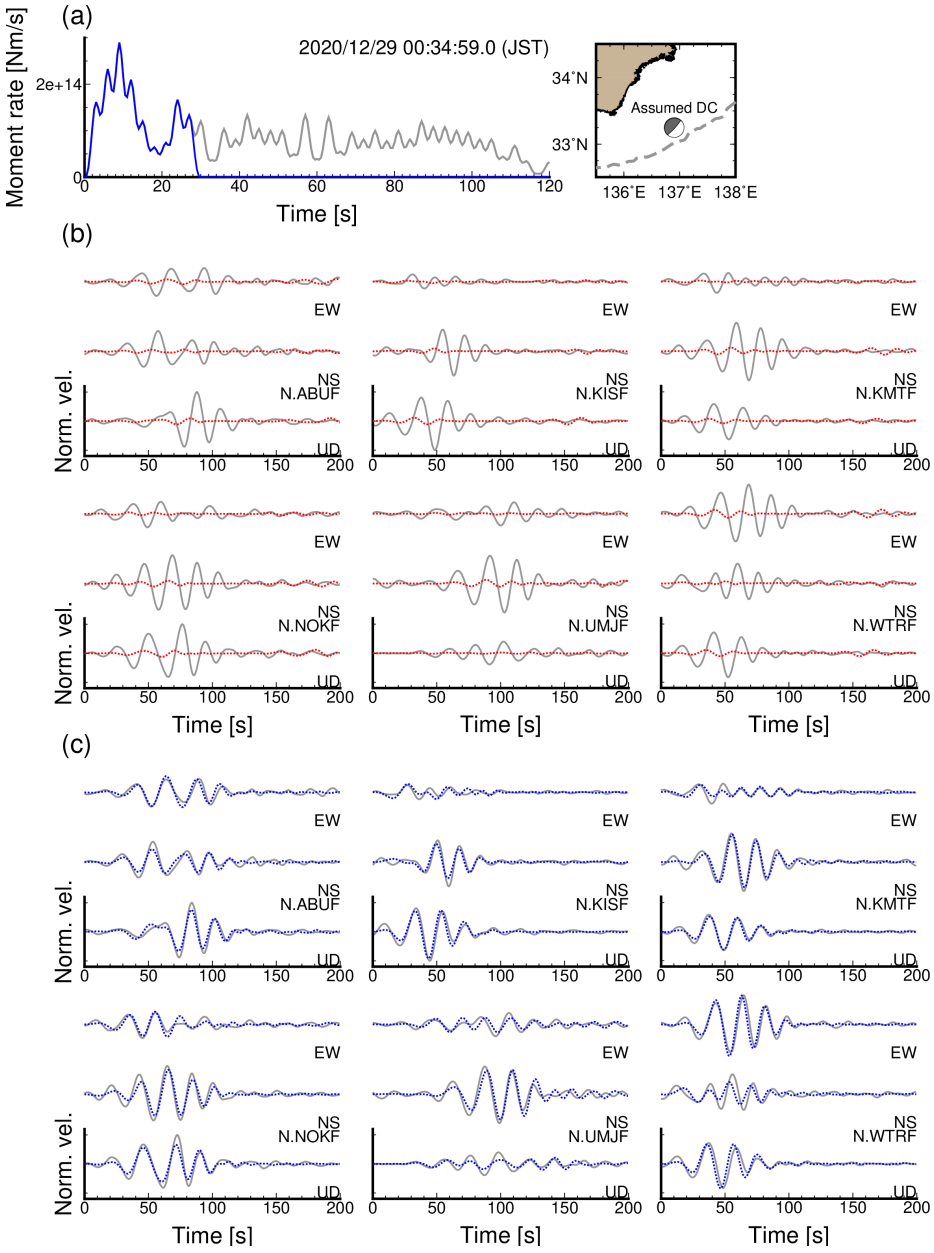

Figure 2. An example of moment rate function estimation for a shallow VLFE that occurred at 00:34:59.0 on 29 December 2020 (JST). (a) Estimated moment rate function, (b) comparisons between observed and initial synthetic waveforms, and (c) comparisons between observed and optimal waveforms. The assumed double-couple (DC) focal mechanism in the map was constructed using the plate geometry of JIVSM (Koketsu et al., 2012) and the convergence direction

of NUVEL-1A (DeMets et al., 2010). Gray and blue lines in (a) are the original estimate and optimal solution of the moment rate function for this shallow VLFE. Observed, initial, and optimal waveforms in (b) and (c) are represented by gray solid, red dotted, and blue dotted lines, respectively. Amplitudes at each station were normalized by the maximum amplitude of observed seismograms at frequencies of 0.02–0.05 Hz for each station.

3 Results

We detected and relocated 2,562 shallow VLFEs from April 2004 to January 2021 (Figure S1). The relationship between seismic moment and duration is illustrated in Figure 3. The results for different VR thresholds are plotted in Figures S4 and S5. Our results (Figure 3b) roughly followed the scaling relations of the slow earthquake family (including LFE, VLFE, and SSE) (e.g., Ide et al., 2007). Sugioka et al. (2012) and Takemura, Matsuzawa, et al. (2019) also estimated the seismic moments and durations of shallow VLFEs in the same region (Figure 3a). Moreover, our estimates (especially those with VRs 50 %) agreed with those of Sugioka et al. (2012) but were systematically larger than those of Takemura, Matsuzawa, et al. (2019). The assumption of a single pulse with various durations was applied in our previous study (Takemura et al., 2018; Takemura, Matsuzawa, et al., 2019). On the other hand, Sugioka et al. (2012) estimated the moment rate functions of shallow VLFEs from temporal ocean bottom seismometer data using a method based on the multiple-pulse assumption. This indicates that the estimation method of moment rate functions based on the single-pulse assumption can capture the centroid of the highest moment release but neglects minor sub-events (Figure S8). Thus, the optimal solutions based on the single-pulse assumption could not reproduce the observed later phases (red lines in Figure S8).

Figure 3c shows the size distribution plot of shallow VLFEs with VRs 30 % assuming a power law (the Gutenberg-Richter law). Our catalog stably contained shallow VLFEs with Mw 3.6. The power law with a b-value of approximately one appeared within the Mw range of 3.7 to 4.1. The number of shallow VLFEs with Mw 4.2 decreased rapidly with increasing Mw. The size distribution characteristics of shallow VLFEs did not change with different VR thresholds in the source time function estimates (Figures S4 and S5). This distribution seems to be a tapered Guttenberg-Richer distribution (e.g., Kagan, 2002; Nakano et al., 2019).

Figure 4a shows the temporal variation in the cumulative moment of shallow VLFEs in the study region. Temporal variations of the cumulative moment from shallow VLFEs with different thresholds (85 % and 95 % of the VR_m) are shown in Figure S6. Owing to template matching and moment rate function estimation based on the multi-pulse assumption, the cumulative moments of the new shallow VLFE catalog were larger than those of Takemura, Matsuzawa, et al. (2019). The total seismic moment released by 17 years of shallow VLFE activity was 2.69×10^{18} Nm (Mw 6.2). Figure 4b shows the spatiotemporal variations of shallow VLFE epicenters along X–X' (strike, 59° from the north)

and Y-Y' (dip) directions. We identified three major episodes (200 shallow VLFEs over a wide area) that started from September 2004, March 2009, and December 2020, respectively. Other minor episodes (10 shallow VLFEs in a limited area) occurred in August 2005, July 2007, March 2008, April 2016, and May 2018. Here, we focus on variations in shallow VLFE activities in the along-strike direction (along X–X' in Figure 4b). Around X of −60 km to −20 km along this section, south-southeast off the Kii Peninsula, shallow VLFEs rarely occurred. In contrast, in regions > 0 km, shallow VLFEs actively occurred. The moment rates of shallow VLFEs in these regions were larger than those in the regions with X < -20 km. Such along-strike variations are illustrated in Figure 5. Figure 5a shows a map view of the cumulative number and moments of shallow VLFEs southeast off the Kii Peninsula. Figure 5b shows the along-strike variations in the durations and moment rates of individual shallow VLFEs. A value of 5×10^{12} Nm/s is suggested as the lowest moment rate of detectable shallow VLFEs at onshore F-net stations. Similar spatial variations were also observed in the solution with 95 % VR_m (Figure S7).

Based on the along-strike variations of shallow VLFE characteristics (Figure 5), we divided the shallow VLFE activity into three regions: Region 1 (−60 km to −20 km), Region 2 (0–35 km), and Region 3 (35–70 km). In Region 1 (blue dashed rectangle and line), shallow VLFE activity was minor, and their moment rates ranged from 5×10^{12} Nm/s to 5×10^{13} Nm/s, which were smaller than those in the other two regions. In Region 2 (red dashed rectangle and line), the shallow VLFEs were the most active. Both the cumulative number and moments were the highest (1,011 and 1.47×10^{18} Nm, respectively). The maximum shallow VLFE moment rates were also the highest (approximately 2×10^{14} Nm/s) in this region. In Region 3 (purple dashed rectangle and line), shallow VLFE activity was also high, but the cumulative number and moments (856 and 1.14×10^{18} Nm) were slightly less than those in Region 2. The maximum moment rates were also slightly lower than those in Region 2.

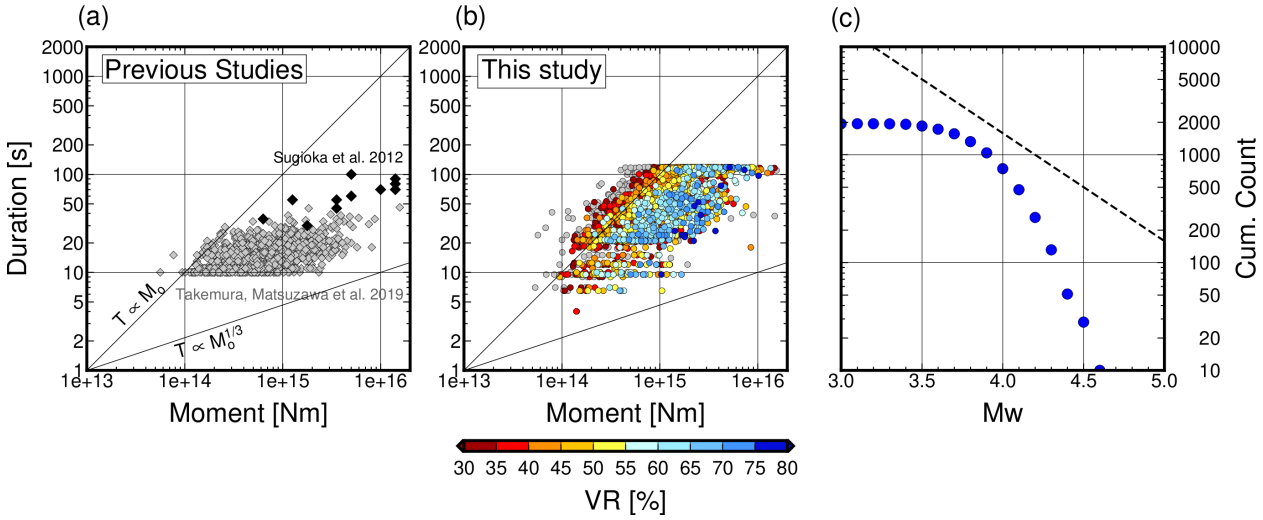

Figure 3. Relationship between seismic moments and durations of shallow VLFEs southeast off the Kii Peninsula. Black and gray diamonds in (a) represent the relationships between seismic moments and durations of shallow VLFEs in Sugioka et al. (2012) and Takemura, Matsuzawa, et al. (2019), respectively. Colors in (b) represent the values of VRs. (c) Size distribution of shallow VLFEs in this study, evaluated from shallow VLFEs with VRs 30 %. Dashed line in (c) represents the Gutenberg-Richter relationship with a b-value of 1.

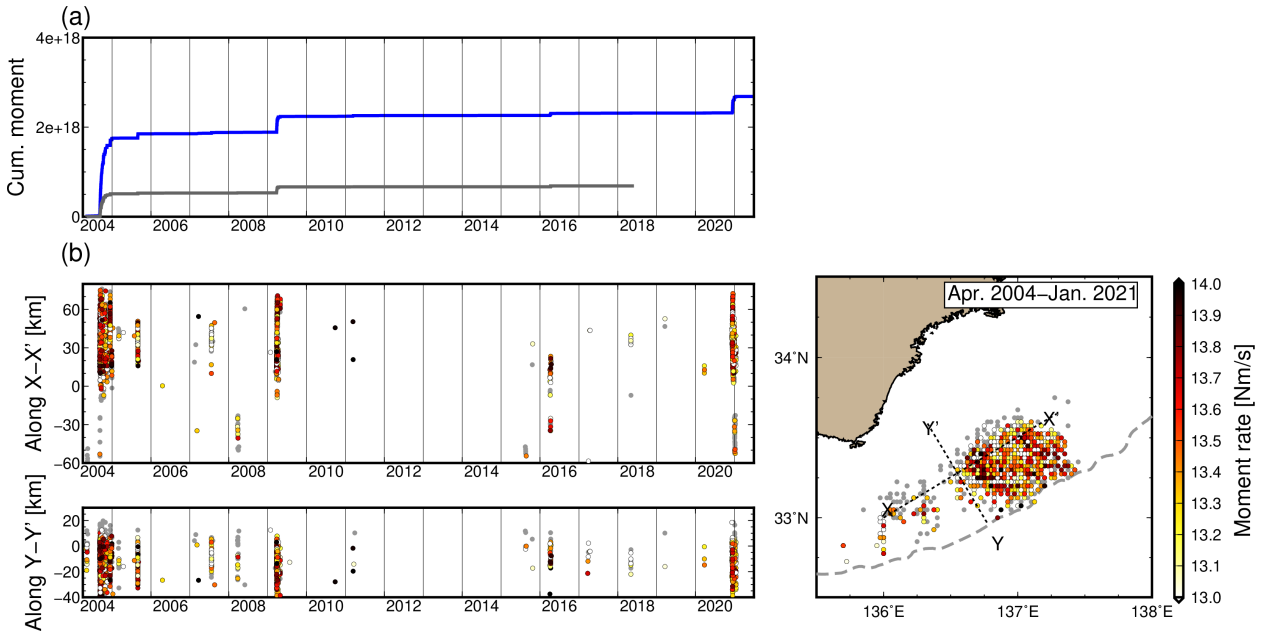

Figure 4. (a) Temporal variations of the cumulative moment and (b) spatiotem-

poral distribution of the moment rate of shallow VLFEs southeast off the Kii Peninsula. Gray and blue lines in (a) are the cumulative moments derived from the catalog in our previous study (Takemura, Matsuzawa, et al., 2019) and this study, respectively. Colors in (b) represent the seismic moments and moment rates of shallow VLFEs with VRs equal to or greater than 30 %. Gray circles represent detected shallow VLFEs with VRs less than 30 %. The intersection point between X-X' and Y-Y' represents X = 0 km and Y = 0 km.

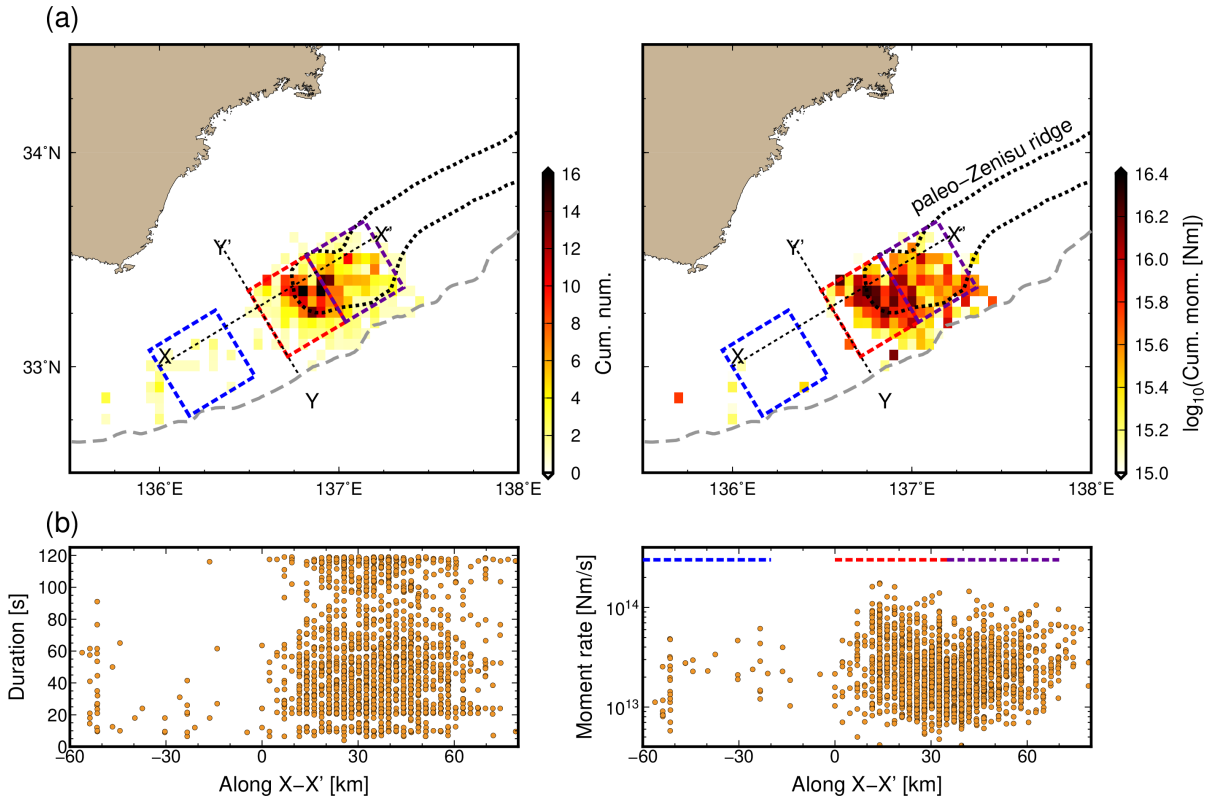

Figure 5. (a) Spatial variations of the block mean values of the cumulative number and moments of shallow VLFEs. We conducted spatial smoothing of the cumulative number and moments of shallow VLFEs within the region of $0.05^{o}\times0.05^{o}$ on the map via the gridding algorithm provided by Generic Mapping Tools (Wessel et al., 2013). Blue, red, and purple dashed rectangles represent Regions 1, 2, and 3, respectively. (b) Along-strike variations in the durations and moment rate of individual shallow VLFEs. Black dotted line represents the location of the paleo-Zenisu ridge (Park et al., 2002, 2004), which is the subducted ridge beneath the study area.

4. Discussion

4.1. Spatial variations of slip behavior on the plate boundary inferred from the estimated source time functions of shallow VLFEs

Various offshore seismic surveys and analysis of DONET waveforms revealed detailed subsurface structures beneath southeast off the Kii Peninsula (e.g., Akuhara et al., 2020; Park et al., 2002, 2004; Tonegawa et al., 2017; Yamamoto et al., 2017). The large coseismic slip of past earthquakes and the spatial variation of interseismic locking in the Nankai Trough have been well studied (e.g., Murotani et al., 2015; Noda et al., 2018). Comparisons with such studies could provide key information for resolving the causes of along-strike variations in shallow VLFE activity in this region. Thus, in this subsection, we compare the observed along-strike variations of shallow VLFE activity with the tectonic environments in this region.

The pore-fluid pressure condition around the plate boundary is an important factor for slow earthquake activity (e.g., Delph et al., 2018; Nakajima & Hasegawa, 2016; Saffer & Wallace, 2015). The pore-fluid pressure is expected to be high within low-velocity volume (e.g., Kitajima & Saffer, 2012). Around regions with strong locking or low pore-fluid pressure, shallow slow earthquakes also tend to be less active (e.g., Baba et al., 2020; Dixon et al., 2014; Nishikawa et al., 2019). Thus, low shallow VLFE activity in Region 1 may be linked to low pore-fluid pressure conditions expected from velocity structures around the plate boundary (e.g., Tonegawa et al., 2017; Yamamoto et al., 2017) and strong interplate locking (e.g., Noda et al., 2018). Based on the observed interplate locking distribution in Nankai, Noda et al. (2021) constructed rupture scenario models for anticipated megathrust earthquakes. In these scenario models, large stress drops and coseismic slips were expected around Region 1. Thus, we consider that shallow slow earthquakes in Region 1 may have a minor contribution to the release of accumulated shear stress due to the subduction of the Philippine Sea Plate.

In Regions 2 and 3, shallow VLFE activity is high. Zones with high V_P/V_S ratios are commonly imaged around the plate boundary (e.g., Akuhara et al., 2020; Tonegawa et al., 2017), indicating that high pore-fluid pressure conditions are expected beneath these regions. Based on multichannel seismic (MCS) reflection profiles (Park et al., 2002, 2004), the paleo-Zenisu ridge (subducted ridge; black dotted line in Figure 5) was confirmed in both Regions 2 and 3. In addition, a décollement zone along the plate boundary was also confirmed beneath the western side of Region 2 from the MCS profile of Park et al. (2002). Thus, a significant change in the geometry of the subducting Philippine Sea Plate exists in Region 2.

The relationship between the subducting ridge and slow earthquakes has been documented in various subduction zones (e.g., Kubo & Nishikawa, 2020; Sun et al., 2020; Todd et al., 2018). The geometry of the Philippine Sea Plate is also related to slow earthquake activity southeast off the Kii Peninsula (e.g., Shiraishi et al., 2020; Toh et al., 2020). Our long-term shallow VLFE catalog revealed the relationship between the shallow VLFE moment releases and topographic features of the Philippine Sea Plate. Wang & Bilek (2011, 2014) pointed out that small earthquakes and aseismic creep in the regions surrounding subducted

seamounts can occur due to the complex structure and heterogeneous stress caused by the subducted seamount. Dehydrated fluid is also heterogeneously distributed around subducted seamounts (e.g., Chesley et al., 2021). Thus, we consider that the paleo-Zenisu ridge causes heterogeneous structure and stress conditions in Regions 2 and 3, thereby promoting the occurrence of shallow slow earthquakes. The slightly higher activity in Region 2 could be related to the significant change in the geometry of the subducting Philippine Sea Plate beneath Region 2 (Park et al., 2002, 2004).

4.2. Variations of shallow VLFE migrations southeast off the Kii Peninsula

According to offshore borehole observation data southeast off the Kii Peninsula, Araki et al. (2017) detected eight shallow SSEs from 2011 to 2016. Ariyoshi et al. (2021) also reported a shallow SSE in March 2020. According to their detections and our shallow VLFE catalog, we observed the simultaneous occurrence of shallow VLFEs and SSEs in March 2011, October 2015, April 2016, and March 2020. Because of the spatiotemporal limitations of offshore geodetic observations (e.g., Araki et al., 2017; Yokota & Ishikawa, 2020), the detailed rupture processes of shallow SSEs cannot be resolved. The migration of tremors and VLFEs may be linked to the rupture processes of SSEs (e.g., Bartlow et al., 2011; Hirose & Obara, 2006; Ito et al., 2007; Rogers & Dragert, 2003). In this subsection, we investigate the spatiotemporal characteristics of shallow VLFE episodes in order to evaluate the possible shallow SSE rupture processes southeast off the Kii Peninsula.

Because our relocated epicenters have relatively large uncertainties along the dip direction owing to the station distribution (Figure 1), we focused our attention on migration patterns along the strike direction. The along-strike migration patterns of shallow VLFE episodes are illustrated in Figures 6, S9, and S10. The episode from September 2004 (Figure S9) was the largest; however, the complicated spatiotemporal variations of shallow VLFEs in this episode might have been affected by the *Mw* 7.4 intraplate earthquake and resulting afterslip that occurred on 5 September, 2004 (e.g., Watanabe et al., 2018). Figure 6 shows the migrations of shallow VLFEs in the episodes that started from March 2009 and December 2020. The cumulative moments during these two episodes were very similar (3.53×10^{17} and 3.67×10^{17} Nm, respectively). Shallow VLFEs with high moment rates were concentrated along the main migration fronts, and several rapid reverse migrations occurred in both episodes. The speed of the observed reverse migrations was approximately 50 km/day, which was slightly slower than the rapid reverse migration of shallow slow earthquakes observed in the Hyuga-nada region (100–200 km/day; Asano et al., 2015; Yamashita et al., 2015). In the episode from March 2009 (upper panel of Figure 6), shallow VLFE activity initiated at approximately 10 km along X–X', and then migrated eastward along the strike direction at a speed of approximately 8 km/day, which is close to the typical migration speeds of the major fronts of shallow slow earthquakes in other regions (e.g., Tanaka et al., 2019) and deep slow earthquakes

(e.g., Houston et al., 2011; Obara, 2010). On the other hand, in the episode from December 2020, shallow VLFE activity initiated at approximately 40 km along X–X', and then bilaterally migrated along the strike direction at a speed of approximately 4 km/day. This activity extended south-southeast off the Kii Peninsula (-50 km along X–X').

We can catch the initiation locations and activity areas of each shallow VLFE episode from Figure 7. The spatiotemporal variations of other minor episodes are illustrated in Figure S10. The shallow VLFEs during the major episodes were commonly concentrated within the same active area (Regions 2 and 3; left panel of Figure 7), although the migration directions and initiation locations in the episode from December 2020 were different. On the other hand, the activity areas of minor episodes, except for that in March 2008, exhibited distinct locations within a part of the major activity area (right part of Figure 7), where the western edge of the paleo-Zenisu ridge exists. Our results suggest that this subducted ridge (black dotted line in Figure 7) also plays an important role in shallow VLFE episodes.

By applying the ambient noise monitoring technique to DONET data from August 2011 to March 2021 (diamonds in Figure 7), Tonegawa et al. (2020) and Tonegawa & Takemura (2021) imaged heterogeneous structural changes associated with shallow slow earthquakes. They interpreted that these structural changes might be caused by fluid migration from the subducting plate, which reduced the effective stress on the plate boundary and promoted the rupture of shallow slow earthquakes. The area exhibiting heterogeneous structural changes in December 2020 (Tonegawa et al., 2020; Tonegawa & Takemura, 2021) agreed well with the area of shallow VLFE activity. Accordingly, we consider that the observed spatiotemporal variations of shallow VLFEs may reflect fluid migration during shallow SSEs in each episode. Tonegawa et al. (2020) and Tonegawa & Takemura (2021) also illustrated various heterogeneous change patterns associated with shallow slow earthquakes. Thus, we interpret that observed variations in the initiation location, migration direction, and area of shallow VLFE episodes reflect temporal changes in the heterogeneous distribution of pore fluid or shear stress on the plate boundary. The heterogeneous temporal activity patterns during minor episodes were also affected by subduction of the paleo-Zenisu ridge. For a more detailed discussion of these processes, future studies should employ high-resolution topographic data of the subducting Philippine Sea Plate and 3D subsurface velocity structure models.

The ambient noise monitoring method at DONET stations is a direct and powerful tool for monitoring fluid migration on the plate boundary; however, the temporal resolution of this method is not high ($>$ one month), compared to the typical durations of shallow slow earthquake episodes (several days to months). In addition, due to the observation period, DONET recorded only one major episode from December 2020 and several minor episodes. Thus, the detailed process of fluid migration during slow earthquakes cannot be fully resolved using this technique. Our spatiotemporal distributions of shallow VLFE migrations

(Figures 6, S9, and S10) can more effectively resolve the detailed process of SSE rupture and fluid migration around the plate boundary. Continuous monitoring and more sophisticated methods for analyzing shallow slow earthquake signals and resolving locations in the along-dip direction can resolve the complexities of these processes in future studies.

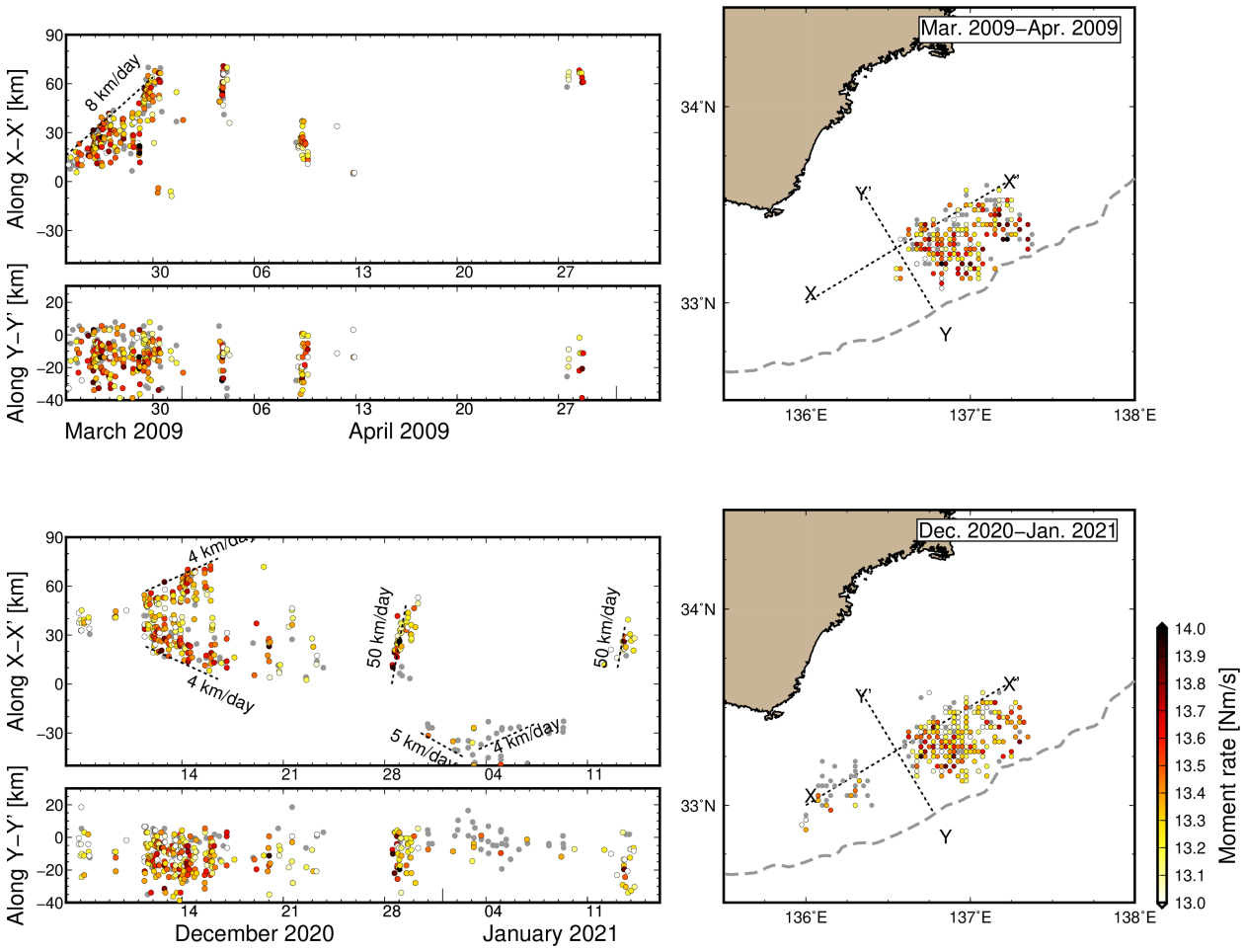

Figure 6. Spatiotemporal distributions of shallow VLFEs during the episodes from (a) March 2009 and (b) December 2020. Colors represent the seismic moments and moment rates of shallow VLFE with VRs 30 %.

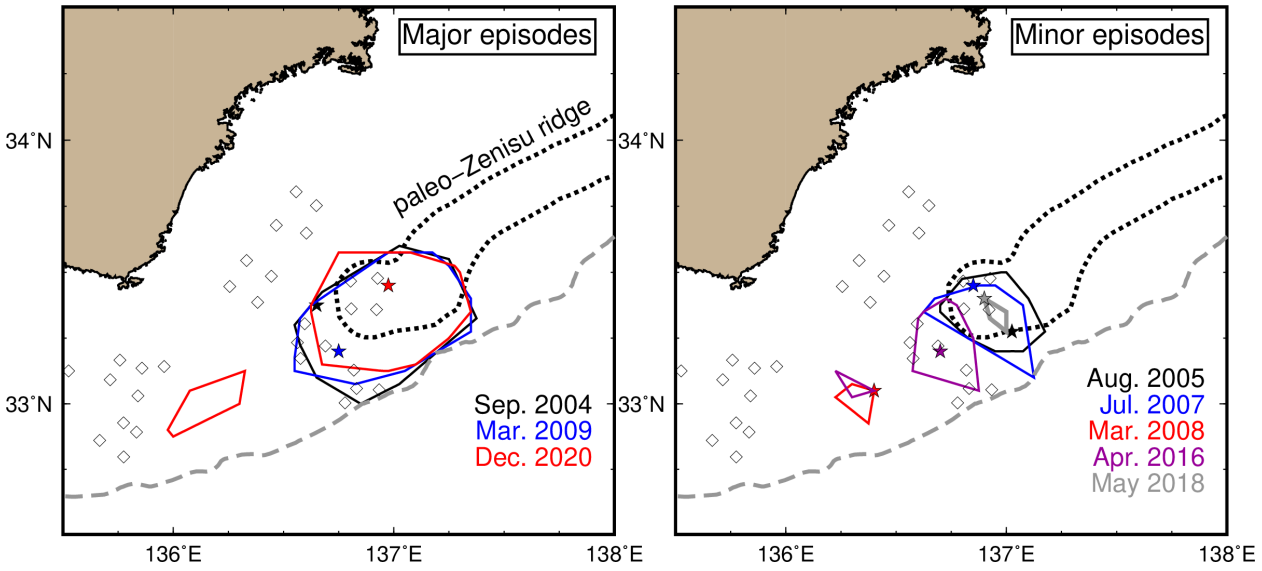

Figure 7. Shallow VLFE activity patterns southeast off the Kii Peninsula. Activity areas are defined by the convex hull of the relocated shallow VLFE epicenters in each episode. Stars indicate the epicenter of the initial shallow VLFE in each episode. Black dotted line represents the location of the paleo-Zenisu ridge (Park et al., 2002, 2004). Diamonds represent the locations of DONET stations.

5. Conclusions

Template matching and relocation based on cross-correlation analysis of onshore broadband records were employed to comprehensively detect shallow VLFEs southeast off the Kii Peninsula along the Nankai Trough. Based on the relocated shallow VLFE locations, we estimated their source time functions using Green's functions in the local 3D model. The estimated source characteristics of shallow VLFEs revealed their spatiotemporal activity patterns in this region. Shallow VLFEs were widely distributed around the accretionary prism toe but exhibited high activity in the region around the western edge of the subducted paleo-Zenisu ridge. This observation suggests that the heterogeneous structure and stress conditions caused by the subduction of the paleo-Zenisu ridge promote the occurrence of shallow VLFEs in this region.

The relocated epicenters illustrated the along-strike migration of shallow VLFEs during three major episodes characterized by a similar activity area and five minor episodes with various activity areas. The major episodes exhibited slow frontal migration with different initiation locations, migration directions, and migration speeds and included several rapid reverse migrations. Minor episodes were distributed in distinct areas within a part of the major episode activity area. According to the characteristics of shallow VLFE episodes and the plate geometry in previous studies, the subducted ridge also plays an important role

in the activity areas of shallow VLFE episodes. Recent developments in monitoring heterogeneous changes from ambient noise wavefields have imaged various areas of heterogeneous change associated with shallow slow earthquakes. Therefore, we conclude that the various migration patterns of shallow VLFE episodes (activity area, speed, and direction) are caused by temporal changes in the pore-fluid pressure or stress conditions on the plate boundary. As such, shallow VLFE monitoring can be an important indicator of these processes.

Acknowledgments

Numerical simulations for evaluating Green's functions were conducted using the Fujitsu PRIMERGY CX600M1/CX1640M1 (Oakforest-PAC) at the Information Technology Center, University of Tokyo. This study was supported by a JSPS KAKENHI Grant-in-Aid for Scientific Research (C), grant number 21K03696, and a Grant-in-Aid for Scientific Research on Innovative Areas "Science of slow earthquakes," grant numbers 19H04626 and JP16H06473. This study was also supported by ERI JURP 2020-S-04 and 2021-S-B102, which provided computational resources for calculating Green's functions. We thank Akiko Takeo, Yojiro Yamamoto, Takashi Tonegawa, Kojiro Tamaribuchi, Masashi Ogiso, Ryo Okuwaki, Takanori Matsuzawa, Akemi Noda, and Kentaro Emoto for useful discussions.

Data availability statement

The Python package HinetPy (Tian, 2020) was used to download NIED F-net continuous records (National Research Institute for Earth Science and Disaster Resilience, 2019). The catalogs of shallow VLFEs from previous studies (Sugioka et al., 2012; Takemura, Matsuzawa, et al., 2019) were downloaded from the Slow Earthquake Database website (Kano et al., 2018; http://www-solid.eps.s.u-tokyo.ac.jp/~sloweq/). We simulated Green's functions in the local 3D model using OpenSWPC version 5.1.0 https://doi.org/10.5281/zenodo.3982232. The 1D layered velocity models of Tonegawa et al. (2017) can be downloaded from https://doi.org/10.5281/zenodo.4158947. The JIVSM (Koketsu et al., 2012) was obtained from https://www.jishin.go.jp/evaluation/seismic_hazard_map/lpshm/12_choshuki_dat/. We used the Seismic Analysis Code (Goldstein & Snoke, 2005; Helffrich et al., 2013) and Generic Mapping Tools (Wessel et al., 2013) for signal processing and figure drawing. Some of the data analysis was conducted using NumPy (Harris et al., 2020), SciPy 1.7.0 (https://doi.org/10.5281/zenodo.5000479), and Pandas 1.2.5 (https://doi.org/10.5281/zenodo.5013202). The estimated moment rate functions of shallow VLFEs southeast off the Kii Peninsula can be downloaded from https://doi.org/10.5281/zenodo.5211090.

References

Akuhara, T., Tsuji, T., & Tonegawa, T. (2020). Overpressured Underthrust Sediment in the Nankai Trough Forearc Inferred From Transdimensional Inversion of High-Frequency Teleseismic Waveforms. *Geophysical Research Letters*, *47*(15), 0–3. https://doi.org/10.1029/2020GL088280Ando,

M. (1975). Source mechanisms and tectonic significance of historical earthquakes along the Nankai trough, Japan. *Tectonophysics*, *27*(2), 119–140. https://doi.org/10.1016/0040-1951(75)90102-XAoi, S., Asano, Y., Kunugi, T., Kimura, T., Uehira, K., Takahashi, N., et al. (2020). MOWLAS: NIED observation network for earthquake, tsunami and volcano. *Earth, Planets and Space*, *72*(1). https://doi.org/10.1186/s40623-020-01250-xAraki, E., Saffer, D. M., Kopf, A. J., Wallace, L. M., Kimura, T., Machida, Y., et al. (2017). Recurring and triggered slow-slip events near the trench at the Nankai Trough subduction megathrust. *Science*, *356*(6343), 1157–1160. https://doi.org/10.1126/science.aan3120Ariyoshi, K., Iinuma, T., Nakano, M., Kimura, T., Araki, E., Machida, Y., et al. (2021). Characteristics of Slow Slip Event in March 2020 Revealed From Borehole and DONET Observatories. *Frontiers in Earth Science*, *8*. https://doi.org/10.3389/feart.2020.600793Asano, Y., Obara, K., Matsuzawa, T., Hirose, H., & Ito, Y. (2015). Possible shallow slow slip events in Hyuganada, Nankai subduction zone, inferred from migration of very low frequency earthquakes, 331–338. https://doi.org/10.1002/2014GL062165.ReceivedBaba, S., Takemura, S., Obara, K., & Noda, A. (2020). Slow earthquakes illuminating interplate coupling heterogeneities in subduction zones. *Geophysical Research Letters*. https://doi.org/10.1029/2020GL088089Baba, S., Obara, K., Takemura, S., Takeo, A., & Abers, G. A. (2021). Shallow Slow Earthquake Episodes Near the Trench Axis Off Costa Rica. *Earth and Space Science Open Archive*. https://doi.org/10.1002/essoar.10505856.1Bartlow, N. M., Miyazaki, S., Bradley, A. M., & Segall, P. (2011). Space-time correlation of slip and tremor during the 2009 Cascadia slow slip event. *Geophysical Research Letters*, *38*(18), 1–6. https://doi.org/10.1029/2011GL048714Bostock, M. G., Thomas, A. M., Savard, G., Chuang, L., & Rubin, A. M. (2015). Magnitudes and moment-duration scaling of low-frequency earthquakes beneath southern Vancouver Island. *Journal of Geophysical Research B: Solid Earth*, *120*(9), 6329–6350. https://doi.org/10.1002/2015JB012195Chesley, C., Naif, S., Key, K., & Bassett, D. (2021). Fluid-rich subducting topography generates anomalous forearc porosity. *Nature*, *595*(7866), 255–260. https://doi.org/10.1038/s41586-021-03619-8Delph, J. R., Levander, A., & Niu, F. (2018). Fluid controls on the heterogeneous seismic characteristics of the Cascadia margin. *Geophysical Research Letters*. https://doi.org/10.1029/2018GL079518DeMets, C., Gordon, R. G., & Argus, D. F. (2010). Geologically current plate motions. *Geophysical Journal International*, *181*(1), 1–80. https://doi.org/10.1111/j.1365-246X.2009.04491.xDixon, T. H., Jiang, Y., Malservisi, R., McCaffrey, R., Voss, N., Protti, M., & Gonzalez, V. (2014). Earthquake and tsunami forecasts: Relation of slow slip events to subsequent earthquake rupture. *Proceedings of the National Academy of Sciences*, *111*(48), 17039–17044. https://doi.org/10.1073/pnas.1412299111Goldstein, P., & Snoke, A. (2005). SAC Availability for the IRIS Community. Retrieved from https://ds.iris.edu/ds/newsletter/vol7/no1/193/sac-availability-for-the-iris-community/Harris, C. R., Millman, K. J., van der Walt, S. J., Gommers, R., Virtanen, P., Cournapeau, D., et al. (2020). Array programming with NumPy. *Na-*

ture, *585*(7825), 357–362. https://doi.org/10.1038/s41586-020-2649-2Helffrich, G., Wookey, J., & Bastow, I. (2013). *The Seismic Analysis Code*. Cambridge: Cambridge University Press. https://doi.org/10.1017/CBO9781139547260Hirose, H., & Obara, K. (2006). Short-term slow slip and correlated tremor episodes in the Tokai region, central Japan. *Geophysical Research Letters*, *33*(17), L17311. https://doi.org/10.1029/2006GL026579Houston, H., Delbridge, B. G., Wech, A. G., & Creager, K. C. (2011). Rapid tremor reversals in Cascadia generated by a weakened plate interface. *Nature Geoscience*, *4*(6), 404–409. https://doi.org/10.1038/ngeo1157Ide, S., Beroza, G. C., Shelly, D. R., & Uchide, T. (2007). A scaling law for slow earthquakes. *Nature*, *447*(7140), 76–79. https://doi.org/10.1038/nature05780Ide, S., Imanishi, K., Yoshida, Y., Beroza, G. C., & Shelly, D. R. (2008). Bridging the gap between seismically and geodetically detected slow earthquakes. *Geophysical Research Letters*, *35*(10), 2–7. https://doi.org/10.1029/2008GL034014Ito, Y., Obara, K., Shiomi, K., Sekine, S., & Hirose, H. (2007). Slow earthquakes coincident with episodic tremors and slow slip events. *Science*, *315*(5811), 503–506. https://doi.org/10.1126/science.1134454Kagan, Y. Y. (2002). Seismic moment distribution revisited: I. Statistical results. *Geophysical Journal International*, *148*(3), 520–541. https://doi.org/10.1046/j.1365-246x.2002.01594.xKano, M., Aso, N., Matsuzawa, T., Ide, S., Annoura, S., Arai, R., et al. (2018). Development of a slow earthquake database. *Seismological Research Letters*, *89*(4), 1566–1575. https://doi.org/10.1785/0220180021Kato, A., Obara, K., Igarashi, T., Tsuruoka, H., Nakagawa, S., & Hirata, N. (2012). Propagation of slow slip leading up to the 2011 Mw9.0 Tohoku-Oki earthquake. *Science*, *335*(6069), 705–708. https://doi.org/10.1126/science.1215141Kato, A., Fukuda, J., Kumazawa, T., & Nakagawa, S. (2016). Accelerated nucleation of the 2014 Iquique, Chile Mw 8.2 Earthquake. *Scientific Reports*, *6*(1), 24792. https://doi.org/10.1038/srep24792Kitajima, H., & Saffer, D. M. (2012). Elevated pore pressure and anomalously low stress in regions of low frequency earthquakes along the Nankai Trough subduction megathrust. *Geophys. Res. Lett.*, *39*, 1–5. https://doi.org/10.1029/2012GL053793Koketsu, K., Miyake, H., & Suzuki, H. (2012). Japan Integrated Velocity Structure Model Version 1. *Proceedings of the 15th World Conference on Earthquake Engineering*, 1–4. Retrieved from http://www.iitk.ac.in/nicee/wcee/article/WCEE2012_1773.pdfKubo, H., & Nishikawa, T. (2020). Relationship of preseismic, coseismic, and postseismic fault ruptures of two large interplate aftershocks of the 2011 Tohoku earthquake with slow-earthquake activity. *Scientific Reports*, *10*(1), 12044. https://doi.org/10.1038/s41598-020-68692-xMaeda, T., Takemura, S., & Furumura, T. (2017). OpenSWPC: an open-source integrated parallel simulation code for modeling seismic wave propagation in 3D heterogeneous viscoelastic media. *Earth, Planets and Space*, *69*(1), 102. https://doi.org/10.1186/s40623-017-0687-2Michel, S., Gualandi, A., & Avouac, J. (2019). Similar scaling laws for earthquakes and Cascadia slow-slip events. *Nature*, *574*(7779), 522–526. https://doi.org/10.1038/s41586-019-1673-6Murotani, S., Shimazaki, K., & Koketsu, K. (2015). Rupture process of the 1946 Nankai earthquake estimated using seismic waveforms and geodetic data. *Journal of Geophysical Research :*

Solid Earth, *120*, 5677–5692. https://doi.org/10.1002/2014JB011676Nakajima, J., & Hasegawa, A. (2016). Tremor activity inhibited by well-drained conditions above a megathrust. *Nature Communications*, *7*, 13863. https://doi.org/10.1038/ncomms13863Nakamura, T., Takenaka, H., Okamoto, T., Ohori, M., & Tsuboi, S. (2015). Long-period ocean-bottom motions in the source areas of large subduction earthquakes. *Scientific Reports*, *5*, 1–2. https://doi.org/10.1038/srep16648Nakano, M., Yabe, S., Sugioka, H., Shinohara, M., & Ide, S. (2019). Event Size Distribution of Shallow Tectonic Tremor in the Nankai Trough. *Geophysical Research Letters*, *46*(11), 5828–5836. https://doi.org/10.1029/2019GL083029National Research Institute for Earth Science and Disaster Resilience. (2019). NIED F-net. https://doi.org/10.17598/NIED.0005Nishida, K. (2017). Ambient seismic wave field. *Proceedings of the Japan Academy, Series B*, *93*(7), 423–448. https://doi.org/10.2183/pjab.93.026Nishikawa, T., Matsuzawa, T., Ohta, K., Uchida, N., Nishimura, T., & Ide, S. (2019). The slow earthquake spectrum in the Japan Trench illuminated by the S-net seafloor observatories. *Science*, *365*(August), 808–813. https://doi.org/10.1126/science.aax5618Noda, A., Saito, T., & Fukuyama, E. (2018). Slip-Deficit Rate Distribution Along the Nankai Trough, Southwest Japan, With Elastic Lithosphere and Viscoelastic Asthenosphere. *Journal of Geophysical Research: Solid Earth*, *123*(9), 8125–8142. https://doi.org/10.1029/2018JB015515Noda, A., Saito, T., Fukuyama, E., & Urata, Y. (2021). Energy-Based Scenarios for Great Thrust-Type Earthquakes in the Nankai Trough Subduction Zone, Southwest Japan, Using an Interseismic Slip-Deficit Model. *Journal of Geophysical Research: Solid Earth*, *126*(5). https://doi.org/10.1029/2020JB020417Obara, K. (2010). Phenomenology of deep slow earthquake family in southwest Japan: Spatiotemporal characteristics and segmentation. *Journal of Geophysical Research: Solid Earth*, *115*(8), 1–22. https://doi.org/10.1029/2008JB006048Obara, K., & Ito, Y. (2005). Very low frequency earthquakes excited by the 2004 off the Kii peninsula earthquakes: A dynamic deformation process in the large accretionary prism. *Earth, Planets and Space*, *57*(4), 321–326. https://doi.org/10.1186/BF03352570Obara, K., & Kato, A. (2016). Connecting slow earthquakes to huge earthquakes. *Science*, *353*(6296), 253–257. https://doi.org/10.1126/science.aaf1512Park, J.-O., Tsuru, T., Kodaira, S., Cummins, P. R., & Kaneda, Y. (2002). Splay fault branching along the Nankai subduction zone. *Science*, *297*(5584), 1157–1160. https://doi.org/10.1126/science.1074111Park, J.-O., Moore, G. F., Tsuru, T., Kodaira, S., & Kaneda, Y. (2004). A subducted oceanic ridge influencing the Nankai megathrust earthquake rupture. *Earth and Planetary Science Letters*, *217*(1–2), 77–84. https://doi.org/10.1016/S0012-821X(03)00553-3Plata-Martinez, R., Ide, S., Shinohara, M., Garcia, E. S., Mizuno, N., Dominguez, L. A., et al. (2021). Shallow slow earthquakes to decipher future catastrophic earthquakes in the Guerrero seismic gap. *Nature Communications*, *12*(1), 3976. https://doi.org/10.1038/s41467-021-24210-9Rogers, G., & Dragert, H. (2003). Episodic tremor and slip on the Cascadia subduction zone: the chatter of silent slip. *Science*, *300*(5627), 1942–1943. https://doi.org/10.1126/science.1084783Saffer, D. M., & Wal-

lace, L. M. (2015). The frictional, hydrologic, metamorphic and thermal habitat of shallow slow earthquakes. *Nature Geoscience*, *8*(8), 594–600. https://doi.org/10.1038/ngeo2490Shiraishi, K., Yamada, Y., Nakano, M., Kinoshita, M., & Kimura, G. (2020). Three-dimensional topographic relief of the oceanic crust may control the occurrence of shallow very-low-frequency earthquakes in the Nankai Trough off Kumano. *Earth, Planets and Space*, *72*(1). https://doi.org/10.1186/s40623-020-01204-3Sugioka, H., Okamoto, T., Nakamura, T., Ishihara, Y., Ito, A., Obana, K., et al. (2012). Tsunamigenic potential of the shallow subduction plate boundary inferred from slow seismic slip. *Nature Geoscience*, *5*(6), 414–418. https://doi.org/10.1038/ngeo1466Sun, T., Saffer, D., & Ellis, S. (2020). Mechanical and hydrological effects of seamount subduction on megathrust stress and slip. *Nature Geoscience*, *13*(March). https://doi.org/10.1038/s41561-020-0542-0Supino, M., Poiata, N., Festa, G., Vilotte, J. P., Satriano, C., & Obara, K. (2020). Self-similarity of low-frequency earthquakes. *Scientific Reports*, *10*(1), 1–9. https://doi.org/10.1038/s41598-020-63584-6Takemura, S., Matsuzawa, T., Kimura, T., Tonegawa, T., & Shiomi, K. (2018). Centroid Moment Tensor Inversion of Shallow Very Low Frequency Earthquakes Off the Kii Peninsula, Japan, Using a Three-Dimensional Velocity Structure Model. *Geophysical Research Letters*, *45*(13), 6450–6458. https://doi.org/10.1029/2018GL078455Takemura, S., Noda, A., Kubota, T., Asano, Y., Matsuzawa, T., & Shiomi, K. (2019). Migrations and Clusters of Shallow Very Low Frequency Earthquakes in the Regions Surrounding Shear Stress Accumulation Peaks Along the Nankai Trough. *Geophysical Research Letters*, *46*(21), 11830–11840. https://doi.org/10.1029/2019GL084666Takemura, S., Matsuzawa, T., Noda, A., Tonegawa, T., Asano, Y., Kimura, T., & Shiomi, K. (2019). Structural Characteristics of the Nankai Trough Shallow Plate Boundary Inferred From Shallow Very Low Frequency Earthquakes. *Geophysical Research Letters*, *46*(8), 4192–4201. https://doi.org/10.1029/2019GL082448Takemura, S., Okuwaki, R., Kubota, T., Shiomi, K., Kimura, T., & Noda, A. (2020). Centroid moment tensor inversions of offshore earthquakes using a three-dimensional velocity structure model: slip distributions on the plate boundary along the Nankai Trough. *Geophysical Journal International*, *222*(2), 1109–1125. https://doi.org/10.1093/gji/ggaa238Takemura, S., Yabe, S., & Emoto, K. (2020). Modelling high-frequency seismograms at ocean bottom seismometers: effects of heterogeneous structures on source parameter estimation for small offshore earthquakes and shallow low-frequency tremors. *Geophysical Journal International*, *223*(3), 1708–1723. https://doi.org/10.1093/gji/ggaa404Tanaka, S., Matsuzawa, T., & Asano, Y. (2019). Shallow Low-Frequency Tremor in the Northern Japan Trench Subduction Zone. *Geophysical Research Letters*, *46*(10), 5217–5224. https://doi.org/10.1029/2019GL082817Tian, D. (2020). HinetPy: A Python package to request and process seismic waveform data from Hi-net. https://doi.org/10.5281/zenodo.3885779Tocheport, A., Rivera, L., & Chevrot, S. (2007). A systematic study of source time functions and moment tensors of intermediate and deep earthquakes. *Journal of Geophysical Research: Solid Earth*, *112*(7), 1–22. https://doi.org/10.1029/2006JB004534Todd, E. K.,

Schwartz, S. Y., Mochizuki, K., Wallace, L. M., Sheehan, A. F., Webb, S. C., et al. (2018). Earthquakes and Tremor Linked to Seamount Subduction During Shallow Slow Slip at the Hikurangi Margin, New Zealand. *Journal of Geophysical Research: Solid Earth*. https://doi.org/10.1029/2018JB016136Toh, A., Chen, W. J., Takeuchi, N., Dreger, D. S., Chi, W. C., & Ide, S. (2020). Influence of a subducted oceanic ridge on the distribution of shallow VLFEs in the Nankai Trough as revealed by moment tensor inversion and cluster analysis, 0–3. https://doi.org/10.1029/2020GL087244Tonegawa, T., & Takemura, S. (2021). Spatio-temporal variation of fluid migration associated with slow earthquakes in the shallow Nankai subduction zone. In *JpGU Meeting 2021*.Tonegawa, T., Araki, E., Kimura, T., Nakamura, T., Nakano, M., & Suzuki, K. (2017). Sporadic low-velocity volumes spatially correlate with shallow very low frequency earthquake clusters. *Nature Communications*, *8*(1), 2048. https://doi.org/10.1038/s41467-017-02276-8Tonegawa, T., Takemura, S., Yabe, S., & Yomogida, K. (2020). Fluid migraion before and during slow earthquakes in the shallow Nankai subduction zones. In *AGU fall meeting*.Vaca, S., Vallée, M., Nocquet, J. M., Battaglia, J., & Régnier, M. (2018). Recurrent slow slip events as a barrier to the northward rupture propagation of the 2016 Pedernales earthquake (Central Ecuador). *Tectonophysics*, *724–725*(November 2017), 80–92. https://doi.org/10.1016/j.tecto.2017.12.012Voss, N., Dixon, T. H., Liu, Z., Malservisi, R., Protti, M., & Schwartz, S. (2018). Do slow slip events trigger large and great megathrust earthquakes ? *Science Advances*, *4*(10), eaat8472.Wang, K., & Bilek, S. L. (2011). Do subducting seamounts generate or stop large earthquakes? *Geology*, *39*(9), 819–822. https://doi.org/10.1130/G31856.1Wang, K., & Bilek, S. L. (2014). Invited review paper: Fault creep caused by subduction of rough seafloor relief. *Tectonophysics*, *610*, 1–24. https://doi.org/10.1016/j.tecto.2013.11.024Watanabe, S., Bock, Y., Melgar, D., & Tadokoro, K. (2018). Tsunami Scenarios Based on Interseismic Models Along the Nankai Trough, Japan, From Seafloor and Onshore Geodesy. *Journal of Geophysical Research: Solid Earth*, *123*(3), 2448–2461. https://doi.org/10.1002/2017JB014799Wessel, P., Smith, W. H. F., Scharroo, R., Luis, J., & Wobbe, F. (2013). Generic mapping tools: Improved version released. *Eos*, *94*(45), 409–410. https://doi.org/10.1002/2013EO450001Yabe, S., Baba, S., Tonegawa, T., Nakano, M., & Takemura, S. (2021). Seismic energy radiation and along-strike heterogeneities of shallow tectonic tremors at the Nankai Trough and Japan Trench. *Tectonophysics*, *800*, 228714. https://doi.org/10.1016/j.tecto.2020.228714Yamamoto, Y., Takahashi, T., Kaiho, Y., Obana, K., Nakanishi, A., Kodaira, S., & Kaneda, Y. (2017). Seismic structure off the Kii Peninsula, Japan, deduced from passive- and active-source seismographic data. *Earth and Planetary Science Letters*, *461*, 163–175. https://doi.org/10.1016/j.epsl.2017.01.003Yamashita, Y., Yakiwara, H., Asano, Y., Shimizu, H., Uchida, K., Hirano, S., et al. (2015). Migrating tremor off southern Kyushu as evidence for slow slip of a shallow subduction interface. *Science*, *348*(6235), 676–679. https://doi.org/10.1126/science.aaa4242Yokota, Y., & Ishikawa, T. (2020). Shallow slow slip events along the Nankai Trough detected by GNSS-A. *Science*

Advances, *6*(3), eaay5786. https://doi.org/10.1126/sciadv.aay5786